Application of Quantum Machine Learning in a Higgs Physics Analysis at the CEPC

Author 1[a,c,*], Author 2[a], Author 3[b], Author 4[b], Author 5[c], Author 6[a] and Author 7[b,*]

[a]Institute of High Energy Physics, University of Chinese Academy of Sciences, 19B Yuquan Road, Shijingshan District, Beijing 100049, China
[b]State Key Laboratory of Nuclear Physics and Technology, Peking University, Beijing 100871, China

ARTICLE INFO

Keywords:
Quantum computing
High Energy Physics
Machine Learning

ABSTRACT

Machine learning has blossomed in recent decades and has become essential in many fields. It significantly solved some problems for particle physics—reconstruction, particle identification, event classification, etc. However, it is now time to break the limitation of conventional machine learning with quantum computing. A support vector machine algorithm with a quantum kernel estimator (QSVM-Kernel) leverages high-dimensional quantum state space to identify a signal from backgrounds. In this study, we have employed this quantum machine learning algorithm to study the $e^+e^- \to ZH$ process at the CEPC (Circular Electron-Positron Collider), a Higgs factory proposed by China. Using 6-qubits on quantum computer simulators, we have optimized the QSVM-Kernel algorithm and obtained a similar classification performance to the classical support-vector machine algorithm. We have also validated the QSVM-Kernel algorithm using 6-qubits on quantum computer hardware from both IBM and Origin (a quantum technology company in China), where the classification performance is approaching noiseless quantum computer simulators. Our study is one of the few examples that apply state-of-the-art quantum computing technologies to particle physics, fundamental science that relies on big experimental data.

1. Introduction

The discovery of the Higgs boson [1, 2] by the ATLAS and CMS experiments at the Large Hadron Collider (LHC) in 2012 was a significant milestone in particle physics. It confirmed the fundamental particle spectrum of the Standard Model and opened a new way to refine our understanding of particle physics. Since then, the LHC experiments have performed extensive studies on the Higgs boson properties: clues for new physics would emerge if any measurement disagrees with the Standard Model prediction. Furthermore, Higgs factories based on lepton colliders have been proposed to perform more precise measurements of the Higgs boson properties and study the deeper structure of particle physics. The Circular Electron-Positron Collider (CEPC), presented by Chinese scientists, is one such collider that acts as a Higgs factory. It will be located in a tunnel with a circumference of approximately 100 km colliding electron-positron pairs at a centre-of-mass energy of up to 250 GeV.

Machine learning has enjoyed widespread success in detector simulation, particle reconstruction and data analyses of experimental particle physics and dramatically enhances the ability to achieve physics discovery. For instance, machine learning algorithms are used in ATLAS and CMS experiments to help separate signals from backgrounds in the observation of the Higgs boson production in association with a top quark pair ($t\bar{t}H$), which directly establishes the Higgs boson couplings to the top quarks [3, 4].

Another essential tool for experimental particle physics could be quantum machine learning. It uses quantum computing to perform machine learning tasks that tackle large data dimensions. Quantum machine learning enables effective operations in high-dimensional quantum state spaces where computers operate with qubits instead of classical bits. Therefore, it could provide fast computing speed and better learning ability than classical machine learning. As an example of quantum machine learning, a support-vector machine algorithm with a quantum kernel estimator (QSVM-Kernel) [5, 6] encodes classical data into quantum state space and makes accurate classifications for certain artificial data sets.

In recent years, the field of quantum computing has developed rapidly. Superconducting quantum and optical quantum computers have been successfully fabricated and have demonstrated capabilities far beyond today's supercomputers in certain computing tasks [7, 8]. In the following decades, this field will likely increase the number of qubits, improve execution time, and reduce device noise for quantum computers. These developments will lay a foundation for the practical application of quantum computing.

Studying quantum machines to utilize the potential of quantum advantage for future particle physics research is important. There have already been proof-of-principle studies that apply quantum machine learning algorithms to detector simulation, particle reconstruction and data analyses. For example, the QSVM-Kernel algorithm has been employed in a few physics analyses at the LHC using both quantum computer simulators and superconducting quantum computer hardware [9, 10, 11]. This study confirms that the quantum machine learning algorithm has the ability to separate signals from backgrounds for certain realistic physics data sets. However, further improvements on both quantum algorithms and quantum devices are still required before the actual use of quantum machine learning in particle physics experiments.

In this study, we focus on applying the QSVM-Kernel al-

*Corresponding author
Author 1@mail (A. 1); Author 7@mail (A. 7)
ORCID(s): ORCID (A. 1)

gorithm to a physics analysis that measures ZH (the Higgs boson production in association with a Z boson) at the CEPC. Using quantum computer simulators, we pursue quantum algorithm designs more suitable for particle physics data analyses. On the other hand, we validate the performance of the QSVM-Kernel algorithm using superconducting quantum computer hardware provided by IBM and Origin Quantum, a quantum technology company in China. We expect improved quantum machine learning algorithms and quantum computer hardware could facilitate physics discovery in the exciting data planned to be produced by the CEPC.

2. Physics Analysis

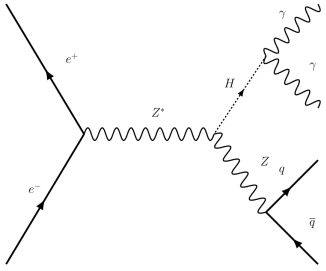

Figure 1: Representative Feynman diagrams for the $e^+e^- \to ZH \to q\bar{q}\gamma\gamma$ production.

The CEPC will operate at a centre-of-mass energy of about 250 GeV where the Higgs boson production cross-section reaches maximum through the $e^+e^- \to ZH$ process. Over one million Higgs bosons will be produced with an integrated luminosity of 5.6 ab^{-1}. These large statistics and the clean final states of electron-positron collisions will allow the CEPC experiments to measure the Higgs boson properties with precision far beyond that at the LHC. $e^+e^- \to ZH$ events can be tagged using the mass of the system recoiling against the Z boson ("recoil mass"), calculated using the difference between the electron-positron pair's four momentum and the Z boson's four momentum. Combining this method with measurements in individual Higgs decay channels will allow for model-independent measures of both $e^+e^- \to ZH$ production cross section and Higgs decay branching ratios, which is not feasible at the LHC. These measurements will extract information on Higgs boson couplings to other fundamental particles and provide sensitive probes to physics beyond the Standard Model.

In our study, we focus on the $H \to \gamma\gamma, Z \to q\bar{q}$ decay mode of the $e^+e^- \to ZH$ process. See Figure 1 for a representative Feynman diagram for this process. Although the diphoton decay of the Higgs boson has a small branching ratio in the SM, the two photons can be well identified and measured, which boosts the precision in this channel. Events are required to have two photon candidates retained as the $H \to \gamma\gamma$ candidate and two jets retained as the $Z \to q\bar{q}$ candidate. The leading photon candidate is required to have energy greater than 35 GeV, the sub-leading photon candidate is required to have energy greater than 25 GeV, and both are required to have polar angles of $|\cos\theta| < 0.9$. Jets are required to have polar angles of $|\cos\theta| < 0.9$. The main SM background process in this analysis is the $e^+e^- \to (Z/\gamma^*)\gamma\gamma$ process where the γ's originate from initial or final state radiation.

The Higgs signal and the SM background events are generated with WHIZARD-1.95 [12] and fast simulated with the CEPC baseline detector design [13]. One can find more details about the event generation on Ref [14].

To reduce the size of the background, we first do some pre-selections. The transverse momentum of each photon has to be larger than 20 GeV and the diphoton invariant mass is required to fall within a broad mass window of 110 GeV $< m_{\gamma\gamma} <$ 140 GeV. To separate signal from background after pre-selections, we construct classifiers based on (either classical or quantum) machine learning algorithms. The kinematic features utilized by these classifiers include: the azimuthal separation between the two photons $\Delta\phi(\gamma\gamma)$, the minimum angular distance between a photon and a jet $min(\Delta R(\gamma, j))$, energy of the diphoton system $e_{\gamma\gamma}$, the momentum of the diphoton system $p_{\gamma\gamma}$, difference in the momentum between the diphoton system and dijet system $\Delta P_{\gamma\gamma,jj}$, and recoil mass of the dijet system M^{jj}_{recoil}. The outputs of these classifiers can be used to create event categories and therefore improve the analysis sensitivity.

3. Quantum algorithm

The support-vector machine (SVM) algorithm [15, 16] with various kernel estimators has been one of the best-known machine learning algorithms for classification problems, such as identifying a small signal from large backgrounds. A quantum version of the SVM algorithm with a quantum kernel estimator (QSVM-Kernel) [5, 6] was proposed to leverage high-dimensional quantum state space for identification accuracy and computational speed. This QSVM-Kernel algorithm is employed and investigated in our study. Conceptually, the training phase of this algorithm can be divided into three following steps.

3.1. Mapping classical datasets

For each classical data point in the training sample, we use $\vec{x}$ to denote the vector of its kinematic features and use $y \in \{-1, 1\}$ to denote its event class (-1 for backgrounds and 1 for the signal). The QSVM-Kernel algorithm maps $\vec{x}$ to a quantum state of N qubits, which is a superposition of 2^N eigenstates. All the N qubits are in the $|0\rangle$ state. A quantum feature map circuit $\mathcal{U}_{\Phi(\vec{x})}$, which represents a unitary transformation, is applied to the N qubits and results in a new quantum state:

$$\left|\Phi(\vec{x})\right\rangle = \mathcal{U}_{\Phi(\vec{x})} \left|0^{\otimes N}\right\rangle \tag{1}$$

The quantum feature map circuit decides how the 2^N dimensional quantum state space will be utilized and the choice of the circuit is essential for the performance of the QSVM-Kernel algorithm. The quantum feature map $\mathcal{U}_{\Phi(\vec{x})}$ in our study, shown in Figure 2 (a), is constituted by single-qubit

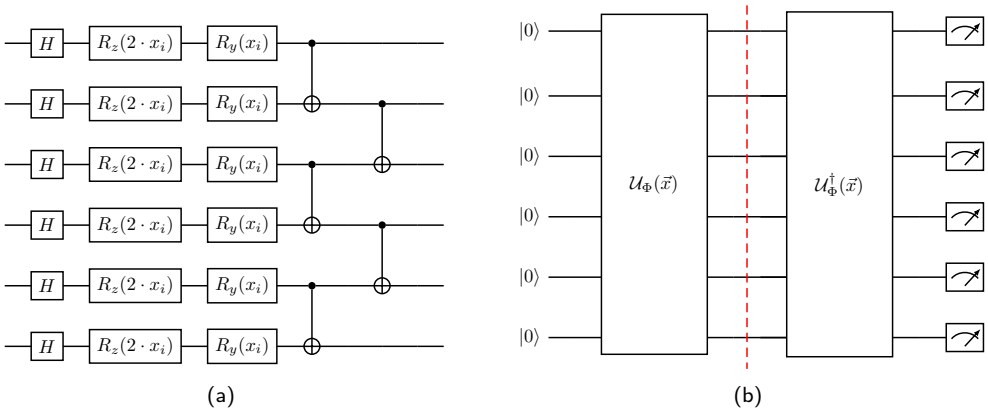

Figure 2: (a) Quantum circuit of the quantum feature map $\mathcal{U}_{\Phi(\vec{x})}$ in our study. It is constituted by single-qubit rotation gates (H, R_z and R_y) and two-qubit CNOT entangling gates. (b) Quantum circuit for evaluating the kernel entry for data events $\vec{x}$ in our study.

rotation gates (H, R_z and R_y) and two-qubit CNOT entangling gates. Given an input feature vector $\vec{x}$ (where x_k denotes the k^{th} element of $\vec{x}$), the k^{th} qubit will be sequentially rotated by an Hadamard (H) gate to the $\frac{|0\rangle+|1\rangle}{\sqrt{2}}$ state, rotated by a R_z gate for $2 \cdot x_k$ around the z-axis of the Bloch sphere, and rotated by a R_y gate for x_k around the y-axis. To avoid long-depth circuits on noisy intermediate scale quantum computers, CNOT entangling gates (which operate the target qubits according to the state of the control qubits) are arranged in an alternating manner: in the first layer, the k^{th} CNOT gate takes the $2 \cdot k - 1$ qubit as the control qubit and takes the $2 \cdot k$ qubit as the target qubit; and in the second layer, the k^{th} CNOT gate takes the $2 \cdot k$ qubit as the control qubit and takes the $2 \cdot k + 1$ qubit as the target qubit.

3.2. Quantum Kernel estimation

The QSVM-Kernel algorithm defines the "kernel entry" between any two data points $\vec{x}_i$ and $\vec{x}_j$ as the square of the inner product of their quantum states:

$$k(\vec{x}_i, \vec{x}_j) = \left| \left\langle \Phi(\vec{x}_i) \right| \Phi(\vec{x}_j) \right\rangle \Big|^2 . \tag{2}$$

The mathematical implication of the kernel entry is the distance between the two data points in the high-dimensional quantum state space. It can be shown that

$$k(\vec{x}_i, \vec{x}_j) = \left| \left\langle 0^{\otimes N} \right| \mathcal{U}^\dagger_{\Phi(\vec{x}_i)} \mathcal{U}_{\Phi(\vec{x}_j)} \left| 0^{\otimes N} \right\rangle \right|^2 . \tag{3}$$

Therefore the kernel entry can be calculated using N qubits on a quantum computer, by preparing the $\mathcal{U}^\dagger_{\Phi(\vec{x}_i)} \mathcal{U}_{\Phi(\vec{x}_j)} \left| 0^{\otimes N} \right\rangle$ state and measuring it on a standard basis with a sufficient number of measurement shots. The frequency of obtaining the $|0^{\otimes N}\rangle$ state in the measurement outputs is taken as the value of the kernel entry. Except the $\mathcal{U}_{\Phi(\vec{x})}$ design, the quantum circuit for calculating the kernel entries is the same as Ref [5] and given in Figure 2 (b).

3.3. Finding separating hyperplane

Using the kernel entries, the QSVM-Kernel algorithm looks for a hyperplane that separate signal from background in the quantum state space:

$$\left(\sum_{i=1}^{t} \alpha_i y_i k(\vec{x}_i, \vec{x}) + b \right) = 0 \tag{4}$$

where t is the size of the training dataset, i is the index of the training data points, and (α_i, b) are parameters to be optimized. The optimization of the separating hyperplane takes the same procedure as for the classical SVM, and is done in a classical computer.

In the testing phase of the QSVM-Kernel algorithm, given any new data point $\vec{x}'$, the kernel entry between $\vec{x}'$ and each training data point is calculated on a quantum computer. Then, on a classical computer and as for the classical SVM, the data point $\vec{x}'$ is classified as "signal" or "background" based on the separating hyperplane, i.e. the sign of $(\sum_{i=1}^{t} \alpha_i y_i k(\vec{x}_i, \vec{x}') + b)$. In addition, the probability for the data point $\vec{x}'$ to be in the signal class can be evaluated and used as a continuous discriminant.

4. Results from Quantum Computer Simulators

We employ the QSVM-Kernel algorithm using 6-qubits on the *StatevectorSimulator* from the IBM Quantum framework [17] and the *Tensor Network Simulator* from the Origin QPANDA framework [18]. Running on classical computers, these tools simulate quantum computers by computing the wavefunction of the qubits as the quantum gates are executed, and outputs the "true" probabilities for each eigenstate when measurements are performed. In our usage of the quantum computer simulators, hardware noises are not considered. These choices lead to reasonable computational speed that allows us to explore large datasets. For a $e^+e^- \to ZH$ analysis dataset of size M, we prepare $\frac{1}{2}M$ simulated

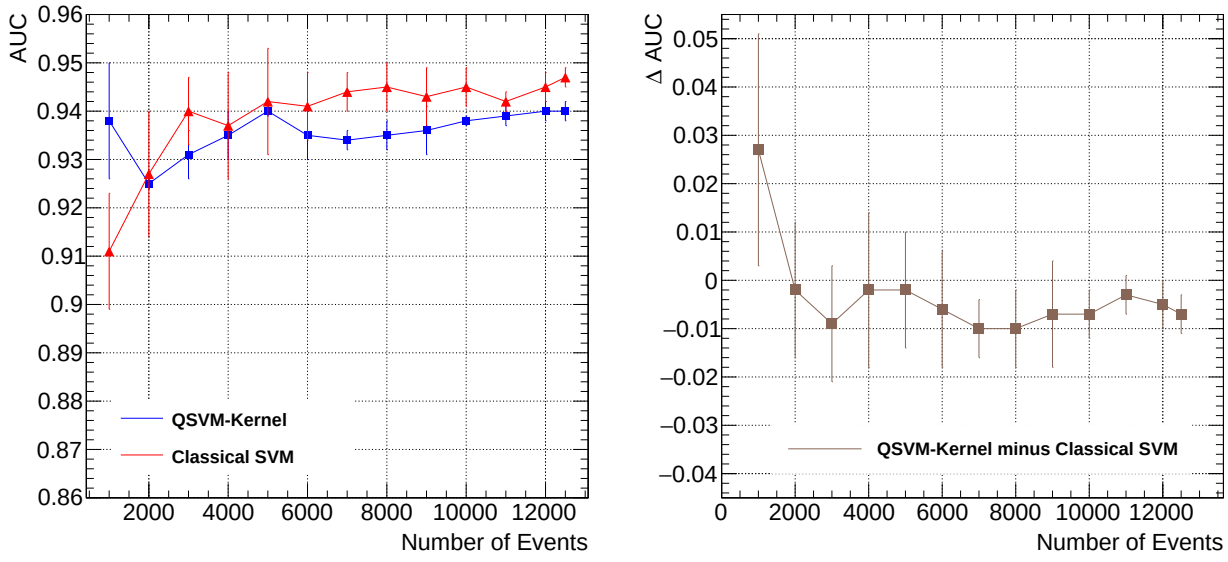

(a) (b)

Figure 3: The AUCs of the QSVM-Kernel and classical SVM classifiers for the $e^+e^- \to ZH$ analysis with different dataset sizes from 1000 to 12500 events. Figure (a) overlays the AUC results of the QSVM-Kernel and the classical SVM as a function of the dataset size. Figure (b) shows the difference in AUC between the QSVM-Kernel algorithm and the classical SVM algorithm, again as a function of the dataset size. The quoted AUCs are the mean for the AUCs of several shuffles for the dataset and the quoted errors are the standard deviations for the AUCs of the shuffles.

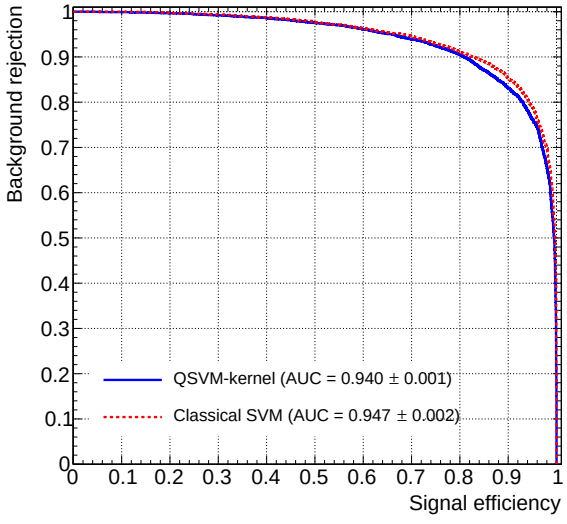

Figure 4: ROC curves of machine learning classifiers using the $e^+e^- \to ZH$ analysis dataset with 12500 events. The plot overlays the results of the QSVM-Kernel algorithm (blue) and classical SVM algorithm (red).

signal events and $\frac{1}{2}M$ simulated background events. We split the analysis dataset into a training sample and a test sample: the training sample consists of $\frac{1}{3}M$ simulated signal events and $\frac{1}{3}M$ simulated background events, and the test sample consists of $\frac{1}{6}M$ simulated signal events and $\frac{1}{6}M$ simulated background events. To evaluate the statistical fluctuation level, we perform this splitting several times, train and test a QSVM-Kernel classifier for each shuffle, and report the average and variation of the results. The SVM regularization hyperparameter for QSVM-Kernel is optimized using a cross-validation procedure [19, 20]. With the same datasets, a classical SVM [15, 16] classifier with the RBF kernel is trained using the scikit-learn package [21], which serves as the classical counterpart for the QSVM-Kernel classifier. Using the same cross-validation procedure as for QSVM-Kernel, we extensively optimize the SVM regularization hyperparameter and the RBF kernel's γ parameter.

We first build QSVM-Kernel and classical SVM classifiers for a $e^+e^- \to ZH$ analysis dataset of 12500 events. To study the performance of the machine learning-based models, we plot Receiver Operating Characteristic (ROC) curves, which show background rejection (in y-axis) as a function of signal efficiency (in x-axis) using the continuous discriminants of the classifiers. The ROC curves for the QSVM-Kernel algorithm (blue) and the classical SVM algorithm (red) are overlaid in Figure 4. The IBM *StatevectorSimulator* and the Origin *Tensor Network Simulator* produce identical ROC curves and are therefore shown together. Additionally, we calculate the areas under the ROC curves (AUCs) for the classifiers, which is a quantitative metric for evaluating the performances of machine learning applications. The AUC of the QSVM-Kernel classifier is found to be 0.940 ± 0.001, compared to 0.947 ± 0.002 for the classical SVM classifier.

The comparison with the ROC curves and AUCs indicates that the quantum SVM algorithm provides similar separation power with its classical counterpart in the $e^+e^- \to ZH$ analysis dataset.

Furthermore, we construct QSVM-Kernel and classical SVM classifiers for the $e^+e^- \to ZH$ analysis with different dataset sizes from 1000 to 12500 events. Figure 3 (a) overlays the AUC results of the QSVM-Kernel and the classical SVM as a function of the dataset size. Figure 3 (b) further shows the difference in AUC between the QSVM-Kernel algorithm and the classical SVM algorithm, again as a function of the dataset size. The quoted AUCs are the mean for the AUCs of several shuffles for a dataset and the quoted errors are the standard deviation for the AUCs of the shuffles. As shown in the figure, concerning separating signal from background for the $e^+e^- \to ZH$ analysis, both algorithms improve the performances with larger dataset size, and for up to 12500 events, the QSVM-Kernel algorithm performs similarly to the classical SVM algorithm.

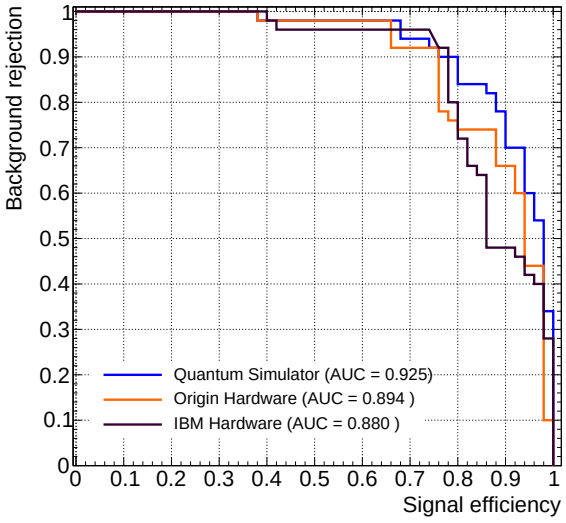

Figure 5: The ROC curves of the QSVM-Kernel classifiers from the IBM Nairobi quantum computer hardware, the Origin Wuyuan quantum computer hardware and the quantum computer simulators with the same $e^+e^- \to ZH$ analysis dataset.

5. Results from Quantum Computer Hardware

In addition to the studies with noiseless quantum computer simulators, we further investigate the QSVM-Kernel algorithm with noisy quantum computer hardware, the 7-qubit Nairobi quantum computer from the IBM company and the 6-qubit Wuyuan quantum computer from the Origin Quantum company. The core of both quantum computers is a superconducting quantum chip system. We employed 6-qubits on both the IBM Nairobi and Origin Wuyuan quantum computers. The topology structures of the qubits in the quantum chip systems are shown in Figure 6. The quantum circuits on the quantum computer hardware are identical to those on the quantum computer simulators. Each quantum circuit was executed and measured 10000 times to allow sufficient statistical precision in evaluating kernel entries. Due to the currently long execution time of the quantum computer hardware, here we analyse a smaller $e^+e^- \to ZH$ analysis dataset consisting of 100 training events and 100 test events. We plot the ROC curves of the QSVM-Kernel clas-

Figure 6: The topology structure of the (a) 7-qubits in the IBM Nairobi and (b) 6-qubits in the Origin Wuyuan quantum chip systems. For (a), our study uses qubit 0, 1, 2, 3, 4, and 5.

sifiers from the IBM Nairobi and Origin Wuyuan quantum computer hardware, as shown in Figure 5. The ROC curve from the *StatevectorSimulator* and *Tensor Network Simulator* with the same $e^+e^- \to ZH$ analysis dataset is overlaid for comparison. The AUC reaches 0.894 from the Origin Wuyuan quantum computer hardware and 0.880 from the IBM Nairobi quantum computer hardware, compared to 0.925 from the quantum computer simulators. We find that the separation power provided by the current quantum computer hardware is approaching that by the noiseless quantum computer simulators. The remaining difference and the difference between IBM Nairobi and Origin Wuyuan results are related to the quantum hardware noises and statistical fluctuations at the time of executing the hardware tasks.

6. Conclusion

In this study, we have employed the QSVM-Kernel algorithm to study the ZH process (Higgs boson production

in association with a Z boson) at the CEPC, a Higgs factory proposed by China for exploring the deeper structure of particle physics. QSVM-Kernel, a quantum machine learning algorithm, can leverage high-dimensional quantum state space for identifying a signal from backgrounds. Using 6-qubits on quantum computer simulators, we optimised the QSVM-Kernel algorithm's quantum circuits for our particle physics data analysis. We obtained a similar classification performance to the classical SVM algorithm with different dataset sizes (from 1000 events to 12500 events). On the other hand, we have validated the QSVM-Kernel algorithm using 6-qubits on superconducting quantum computer hardware from both IBM and Origin (a quantum technology company in China). This validation characterises the classification performance for a small dataset (of 100 events) which approaches noiseless quantum computer simulators. Our study is one of the few examples that apply state-of-the-art quantum computing technologies to particle physics, fundamental science that relies on big experimental data.

Looking toward the future, given the incredible momentum in the field of quantum technology, we expect to see significantly improved quantum machine learning algorithms and quantum computer hardware. With these, particle physicists could better handle high dimensions and large-size physics datasets from future particle colliders, providing possibilities for discovering new fundamental particles and interactions.

Acknowledgements

The authors acknowledge the funding support from the State Key Laboratory of Nuclear Physics and Technology, Peking University (Grant No. NPT2022ZZ05), the funding support by the NSFC Basic Science Center Program for "Joint Research on High Energy Frontier Particle Physics" (Grant No. 12188102), and the funding support by the Science and Technology lnnovation Project of Institute of High Energy Physics Chinese Academy of Sciences (Grand No. E25453U210). The authors acknowledge the computing and data resources provided by computing cernter of Institute of High Energy Physics, National High Energy Physics Data Center and High Energy Physics Data Center, Chinese Academy of Science. The authors thank Dr. Teng Li (Shangdong University) for helpful discussion.

A.F., Q.S. and C.Z. optimized the quantum machine learning algorithm and designed its application to the CEPC physics analysis. A.F., Q.S. and Y.F. produced simulated events for the CEPC physics analysis. A.F., Q.S. and Z.L. produced results on the quantum computer hardware. A.F., Q.S., Y. X. and Y. Z. produced results on the quantum computer simulators. A.F., Q.S., C.L. and S.Q. produced results of the classical machine learning algorithm. C.Z. wrote the initial manuscript. All authors contributed to the revising and reviewing of the manuscript. Y.F. and C.Z. oversaw this study.

References

[1] ATLAS Collaboration, Observation of a new particle in the search for the standard model Higgs boson with the ATLAS detector at the LHC, Physics Letters B 716 (2012) 1–29.

[2] CMS Collaboration, Observation of a new boson at a mass of 125 GeV with the CMS experiment at the LHC, Physics Letters B 716 (2012) 30–61.

[3] ATLAS Collaboration, Observation of Higgs boson production in association with a top quark pair at the LHC with the ATLAS detector, Physics Letters B 784 (2018) 173–191.

[4] CMS Collaboration, Observation of $t\bar{t}H$ production, Physical Review Letters 120 (2018) 231801.

[5] V. Havlíček, A. D. Córcoles, K. Temme, A. W. Harrow, A. Kandala, J. M. Chow, J. M. Gambetta, Supervised learning with quantum-enhanced feature spaces, Nature 567 (2019) 209–212.

[6] M. Schuld, N. Killoran, Quantum machine learning in feature hilbert spaces, Physical Review Letters 122 (2019) 040504.

[7] F. A. et al., Quantum supremacy using a programmable superconducting processor, Nature 574 (2019) 505–510.

[8] H.-S. Z. et al., Quantum computational advantage using photons, Science 370 (2020) 1460–1463.

[9] S. L. Wu, et al., Application of quantum machine learning using the quantum kernel algorithm on high energy physics analysis at the LHC, Physical Review Research 3 (2021) 033221.

[10] K. Terashi, M. Kaneda, T. Kishimoto, M. Saito, R. Sawada, J. Tanaka, Event Classification with Quantum Machine Learning in High-Energy Physics, Comput. Softw. Big Sci. 5 (2021) 2.

[11] J. Heredge, C. Hill, L. Hollenberg, M. Sevior, Quantum Support Vector Machines for Continuum Suppression in B Meson Decays, Comput. Softw. Big Sci. 5 (2021) 27.

[12] W. Kilian, T. Ohl, J. Reuter, WHIZARD: Simulating Multi-Particle Processes at LHC and ILC, Eur. Phys. J. C 71 (2011) 1742.

[13] M. Ahmad, et al., CEPC-SPPC Preliminary Conceptual Design Report. 1. Physics and Detector (2015).

[14] X. Mo, G. Li, M.-Q. Ruan, X.-C. Lou, Physics cross sections and event generation of e^+e^- annihilations at the CEPC, Chin. Phys. C 40 (2016) 033001.

[15] B. Boser, I. Guyon, V. Vapnik, A training algorithm for optimal margin classifiers, Proceedings of the fifth annual workshop on Computational learning theory (1992) 144–152.

[16] C. Cortes, V. Vapnik, Support-vector networks, Machine learning 20 (1995) 273–297.

[17] MD SAJID ANIS and others, Qiskit: An open-source framework for quantum computing, 2021.

[18] Z.-Y. Chen, G.-P. Guo, Qrunes: High-level language for quantum-classical hybrid programming, arXiv preprint arXiv:1901.08340 (2019).

[19] D. M. Allen, The relationship between variable selection and data agumentation and a method for prediction, Technometrics 16 (1974) 125–127.

[20] M. Stone, Cross-validatory choice and assessment of statistical predictions, Journal of the Royal Statistical Society, Series B (Methodological) 36 (1974) 111–147.

[21] F. Pedregosa, et al., Scikit-learn: Machine learning in python, Journal of Machine Learning Research 12 (2011) 2825–2830.